A&A 566, A113 (2014)
DOI: 10.1051/0004-6361/201323345

Astronomy & Astrophysics

The properties of planets around giant stars⋆,⋆⋆

M. I. Jones[1,2], J. S. Jenkins[2], P. Bluhm[3], P. Rojo[2,4], and C. H. F. Melo[5]

[1] Department of Electrical Engineering and Center of Astro-Engineering UC, Pontificia Universidad Católica de Chile, Av. Vicuña Mackenna 4860, 782-0436 Macul, Santiago, Chile
e-mail: mjones@aiuc.puc.cl
[2] Departamento de Astronomía, Universidad de Chile, Camino El Observatorio 1515, Casilla 36-D Las Condes, Santiago, Chile
[3] Departamento de Astronomía, Universidad de Concepción, Casilla 160-C Concepción, Chile
[4] Department of Astronomy, Cornell University, 610 Space Sciences Building, Ithaca NY14853-6801, USA
[5] European Southern Observatory, Casilla 19001 Santiago, Chile

Received 27 December 2013 / Accepted 22 April 2014

ABSTRACT

Context. More than 50 exoplanets have been found around giant stars, revealing different properties when compared to planets orbiting solar-type stars. In particular, they are super-Jupiters and are not found orbiting interior to ~0.5 AU.
Aims. We are conducting a radial velocity study of a sample of 166 giant stars aimed at studying the population of close-in planets orbiting giant stars and how their orbital and physical properties are influenced by the post-MS evolution of the host star.
Methods. We have collected multiepoch spectra for all of the targets in our sample. We have computed precision radial velocities from FECH/CHIRON and FEROS spectra, using the I_2 cell technique and the simultaneous calibration method, respectively.
Results. We present the discovery of a massive planet around the giant star HIP 105854. The best Keplerian fit to the data leads to an orbital distance of 0.81 ± 0.03 AU, an eccentricity of 0.02 ± 0.03 and a projected mass of $8.2 \pm 0.2\ M_J$. With the addition of this new planet discovery, we performed a detailed analysis of the orbital properties and mass distribution of the planets orbiting giant stars. We show that there is an overabundance of planets around giant stars with $a \sim 0.5$–0.9 AU, which might be attributed to tidal decay. Additionally, these planets are significantly more massive than those around MS and subgiant stars, suggesting that they grow via accretion either from the stellar wind or by mass transfer from the host star. Finally, we show that planets around evolved stars have lower orbital eccentricities than those orbiting solar-type stars, which suggests that they are either formed in different conditions or that their orbits are efficiently circularized by interactions with the host star.

Key words. planetary systems – techniques: radial velocities – stars: evolution

1. Introduction

For the past two decades, different methods have been developed to detect and characterize extrasolar planets, giving rise to the discovery of more than 1000 planetary systems. Among them, the radial velocity (RV) technique has led to the detection of a significant fraction of these systems. Unfortunately, this method is strongly sensitive to the spectral properties of the object, and hence it is mainly restricted to solar-type stars. On the one hand, very low-mass stars (such as mid and late M stars) are faint and their spectral distribution peaks in the infrared (IR) region, hence they have been mostly excluded in optical RV surveys. On the other hand, intermediate- and high-mass stars ($M_\star \gtrsim 1.5\ M_\odot$) are too hot and thus they have an optical spectrum that is characterized by few and broad lines. However, after the main-sequence (MS), they expand becoming cooler, and also their rotational velocity is strongly reduced. As a result, their spectra present thousands of narrow absorption lines, becoming suitable targets for precision RV surveys. Therefore, enough RV information can be obtained to search for planets around intermediate-mass stars and to study the dynamical interaction between them and the host star during the giant phase. Unfortunately, giant stars present a high level of jitter (e.g., Sato et al. 2005), limiting the detection only to giant planets ($K \gtrsim 30\ \mathrm{m\,s^{-1}}$).

So far, more than 50 giant planets have been found around giant stars, revealing interesting properties that seem to contrast the properties of giant planets discovered around dwarf stars. First, there is no planet orbiting any giant star in orbits interior to $a \sim 0.5$ AU, in contrast to what is observed in solar-type stars, where there is a large number of discovered close-in gas giants. This observational result suggests that the innermost planets are destroyed by the host star during the expansion phase of the stellar envelope. Moreover, several theoretical studies have shown that the tidal interaction between the planet and the stellar convective envelope leads to the loss of orbital angular momentum. As a result, close-in planets are expected to spiral inward and hence are subsequently engulfed by the host star (e.g., Livio & Soker 1983; Kunitomo et al. 2011). However, Johnson et al. (2007) showed that close-in planets are also absent around intermediate-mass subgiant stars. Additionally, Bowler et al. (2010) confirmed the Johnson et al. findings and also they showed that planets around intermediate-mass stars tend to reside at a larger orbital distance ($a \gtrsim 1$ AU) than planets around solar-type stars. According to these results, planets around giant stars are not found in close-in orbits because of a different formation scenario around intermediate-mass stars instead of a dynamical evolutionary process, such as tidal orbital decay.

Second, the mass distribution of planets around giant stars is different than for planets around dwarf stars. In particular, their

⋆ Based on observations collected at La Silla – Paranal Observatory under programs IDs 085.C-0557, 087.C.0476, 089.C-0524 and 090.C-0345.

⋆⋆ The RV Table is only available at the CDS via anonymous ftp to cdsarc.u-strasbg.fr (130.79.128.5) or via http://cdsarc.u-strasbg.fr/viz-bin/qcat?J/A+A/566/A113

occurrence rate is higher and they are on average more massive (Döllinger et al. 2009). This observational result is supported by theoretical studies that predict an increase in the frequency of giant planets with the mass of the host star (e.g., Kennedy & Kenyon 2008).

Last, planet-hosting giant stars are on average metal-poor, in direct contrast to the well known planet-metallicity connection that is observed in MS stars (Gonzalez 1997; Santos et al. 2001; Fischer & Valenti 2005), which seems to be also present in the low-mass planetary regime (Jenkins et al. 2013a). Following the discussion presented in Schuler et al. (2005), Pasquini et al. (2007) argued that the enhanced metallicity of MS host stars is explained by pollution, instead of being a primordial feature of the protoplanetary disk. In this scenario, a significant amount of material, including planetesimals and planet cores, fall into the star, hence increasing the metal abundance in its atmosphere. However, after these polluted stars evolve off the main-sequence, they develop large convective envelopes, where the metal excess is diluted. This idea might explain the aforementioned discrepancy between MS and giant host stars metallicity distribution. However, more recently, Mortier et al. (2013) showed that RV surveys of giant stars are biased toward metal-poor stars, which explains why planets are preferentially found around metal-poor giants. On the other hand, giant planets around intermediate-mass stars might be efficiently formed by the disk instability mechanism (Boss 1997). In this scenario the metal content of the protoplanetary disk does not play a significant role on the formation of planets, hence it might explain why we do not see a trend toward metal richness in host giant stars.

In this paper, we present the discovery of a massive planet around the red giant branch (RGB) star HIP 105854, as part of the EXoPlanets aRound Evolved StarS (EXPRESS) project (Jones et al. 2011, 2013) and we present a detailed analysis of the properties of exoplanets around post-MS stars. In Sects. 2 and 3, we describe the observations, the data reduction and the RV computation method. In Sects. 4 and 5, we discuss the stellar properties of the host star and the derived orbital parameters of HIP 105854 b. In Sect. 6, we present the line profile analysis and the study of the photometric variability of HIP 105854. In Sect.7, we summarize the properties of the planets detected around giant stars and we discuss the effect of the stellar evolution on these properties. Finally, the conclusions are presented in Sect. 8.

2. A massive planet around the intermediate-mass giant star HIP 105854

2.1. Observations and data reduction

A total of 13 spectra of HIP 105854 were taken on seven different nights using the Fiber-fed Extended Range Optical Spectrograph (FEROS; Kaufer et al. 1999), on the 2.2 m telescope, at La Silla Observatory. FEROS has a mean resolving power of $R \sim 48\,000$, covering the entire optical spectral range. The typical observing time was 70−150 s (depending on the atmospheric conditions), giving rise to a signal-to-noise ratio (S/N) of ∼100−200, at 5500 Å. The spectra were extracted with the FEROS Data Reduction System, which performs a bias subtraction, the flat-field correction, and order extraction. The wavelength solution was computed from a total of ∼1000 emission lines, which are identified in two different ThArNe lamps that were taken either at the beginning of the night, or in the morning, just after the end of the observations. The typical root mean square (rms) in the wavelength calibration is ∼0.005 Å. The barycentric correction performed by the FEROS pipeline was disabled.

Additionally, we obtained 36 spectra using the old fiber echelle spectrograph (FECH) and CHIRON (Tokovinin et al. 2013), both of them installed in the 1.5 m telescope, at The Cerro Tololo Inter-American Observatory. The two spectrographs are equipped with an I_2 cell that is placed in the light beam, which superimposes thousands of narrow absorption lines in the spectral region between ∼5000−6000 Å. The I_2 absorption spectrum was used as a precise wavelength reference (see Sect. 2.2). We used the narrow slit with FECH ($R \sim 45\,000$) and the slit mode with CHIRON ($R \sim 90\,000$). The typical observing time was 700−800 s, leading to a $S/N \gtrsim 50$. The extraction of the data was done in a similar fashion as that for the FEROS spectra, using the automatic reduction pipeline that is offered to CHIRON users. For more details see Jones (2013).

2.2. Radial velocity computations

The radial velocities from the FEROS spectra were computed by applying the simultaneous calibration method (Queloz et al. 1999). The details of the calculations are explained in Jones et al. (2013) and Jones & Jenkins (2014), but the basic ideas of the procedure are also described below.

First, we computed the cross-correlation function (CCF) between the observed spectrum and a template. In this case the template corresponds to a high S/N observation of HIP 105854. We repeated this procedure on chunks of ∼50 Å width (four chunks per order, from 35 different orders). We then used an iterative rejection code to compute the mean radial velocity from all of the chunk velocities. In a similar fashion, we also applied this procedure to the sky fiber, which is illuminated during the science observation by a ThArNe lamp. This method allows us to compute the spectral drift, which is added to the RV measured with respect to the stellar template. Finally, the barycentric velocity is computed and is added to the stellar velocity. It is worth noting that the velocity drift and the barycentric velocity can take either negative or positive values. The typical single shot precision achieved for this star using our code is ∼5 m s^{-1}.

The FECH and CHIRON velocities were computed using the I_2 cell technique (Butler et al. 1996). The basic idea of this method is to pass the stellar light through a cell that contains molecular iodine vapor, which superimposes thousands of absorption lines in the wavelength region between 5000 Å and 6000 Å. These absorption lines are used as wavelength markers against which the spectral doppler shift can be measured. We followed a similar procedure as the one described in Butler et al. (1996), although with some small modifications. For instance, we computed the RVs on chunks of 5 Å (instead of 2 Å) and we used a simpler model for the instrumental point spread function (PSF), including only three Gaussians. We found that this combination of chunk size and PSF modeling yields to the best RV precision, especially for the FECH spectra. We obtained a typical radial velocity precision of ∼11 m s^{-1} for FECH data and ∼6 m s^{-1} using CHIRON spectra. Further details can be found in Jones (2013).

2.3. Stellar properties

HIP 105854 is listed in the Hipparcos catalog as a K2III star, with $B - V$ color equal to 1.20 and visual magnitude of 5.64 The parallax of 12.37 corresponds to a distance of 80.84 parsecs. Based on the equivalent width of more than 100 iron lines, and by imposing local thermodynamic equilibrium, Jones

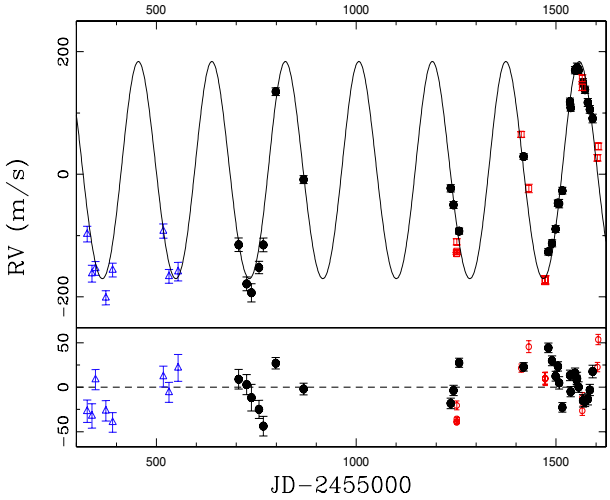

Fig. 1. *Upper panel*: radial velocity curve for HIP 105854. The open blue triangles, black filled dots and red open squares correspond to FECH, CHIRON and FEROS velocities, respectively. The best single-planet solution is overplotted (solid black line). *Lower panel*: residuals from the Keplerian fit. The rms is 23.6 m s^{-1}.

Table 1. Stellar parameters of HIP 105854.

Parameter	Value
Spectral type	K2III
$B-V$ (mag)	1.2
V (mag)	5.64
Parallax (mas)	12.37 ± 0.31
Distance (pc)	80.84 ± 2.03
$T_{\rm eff}$(K)	4780 ± 100
log L ($L_\odot$)	1.670 ± 0.046
log g (cm s^{-1})	2.94 ± 0.20
[Fe/H] (dex)	0.31 ± 0.18
$M_\star$ ($M_\odot$)	2.1 ± 0.1

et al. (2011) derived the following atmospheric parameters for HIP 105854: $T_{\rm eff}$ = 4780 ± 100 K, log L = 1.670 ± 0.046 $L_\odot$, log g = 2.94 ± 0.20 cm s^{-1} and [Fe/H] = 0.31 ± 0.18 dex. It is worth mentioning that the photometric and spectroscopic values of logg are systematically different (see discussion in Jones et al. 2011). By comparing these quantities with Salasnich et al. (2000) evolutionary tracks, they identified this object as a post-RGB star with $M_\star$ = 2.1 ± 0.1 $M_\odot$. These values are summarized in Table 1.

2.4. Orbital parameters of HIP 105854 b

For the past three years, we have collected a total of 49 high resolution and high S/N spectra of the evolved star HIP 105854, using three different instruments, namely FECH, CHIRON and FEROS. From these datasets we measured precision RV variations, which have revealed a large amplitude periodic signal. Figure 1 shows the radial velocity curve of HIP 105854. The blue open triangles and black filled dots correspond to FECH and CHIRON velocities, respectively, whereas the red open squares to FEROS RVs. The FEROS and FECH/CHIRON radial velocity variations are listed in Tables 2 and 3, respectively[1]. The solid line corresponds to the best Keplerian fit including only one planet. The solution was computed with the Systemic console (Meschiari et al. 2009). The uncertainties in the orbital parameters were estimated using the bootstrap randomization method. The residuals of the fit are plotted in the lower panel. The rms is 23.6 m s^{-1}, which is consistent with the amplitude of stellar oscillations observed in giant stars (e.g., Frink et al. 2001). However, it seems that there is also a long term linear trend in the residuals, suggesting the presence of a distant stellar companion. By including a linear trend, the best solution leads

[1] The RVs are relative to the mean values of the two datasets. There is also a zero point offset between the FEROS and FECH/CHIRON velocities.

Table 2. FEROS radial velocity variations of HIP 105854.

JD – 2 455 000	RV (m s^{-1})	error (m s^{-1})
1251.540	–64.1	5.0
1251.597	–82.4	1.7
1251.600	–79.6	1.9
1251.602	–83.4	1.6
1412.805	111.0	4.6
1431.821	22.9	6.7
1472.822	–126.1	6.6
1472.853	–127.0	7.2
1472.890	–126.1	6.8
1565.558	202.5	5.7
1565.615	187.8	5.4
1603.591	72.8	5.2
1605.623	91.6	5.7

Table 3. FECH/CHIRON radial velocity variations of HIP 105854.

JD – 2 455 000	RV (m s^{-1})	error (m s^{-1})
326.900	–68.1	12.6
338.851	–133.8	13.7
347.865	–125.4	11.3
373.746	–173.0	11.5
390.762	–129.5	11.1
517.551	–65.4	11.6
531.553	–139.0	11.2
554.519	–131.7	15.1
705.838	–86.0	11.0
725.866	–150.4	11.2
737.903	–163.9	14.9
756.807	–125.2	10.1
767.798	–86.6	11.1
798.755	163.0	6.4
868.494	18.5	6.6
1236.531	5.1	5.9
1243.537	–21.8	5.7
1257.551	–64.8	5.1
1418.928	57.8	4.8
1480.818	–98.4	5.4
1489.911	–84.4	5.6
1498.898	–61.3	5.6
1504.699	–18.8	5.3
1507.754	–19.6	7.0
1515.805	1.2	5.4
1534.849	146.6	5.9
1536.687	136.2	5.7
1547.655	197.7	5.8
1551.601	199.0	5.1
1552.541	201.6	7.1
1556.527	196.8	5.9
1567.496	177.2	6.9
1572.499	166.4	5.9
1579.517	145.9	6.6
1584.530	134.3	6.3
1591.523	119.6	7.1

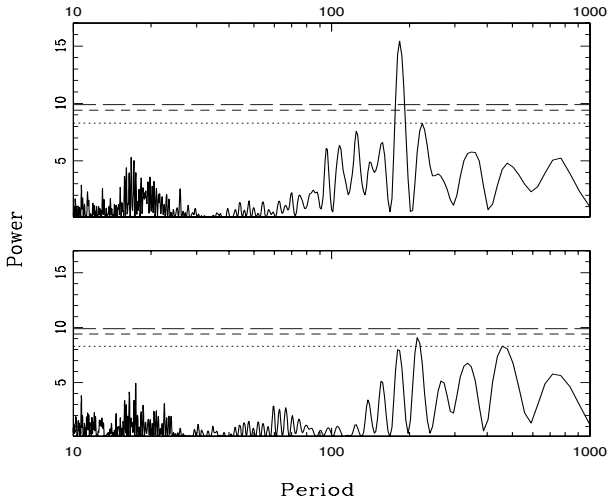

Fig. 2. LS periodogram of the HIP105854 radial velocities (*upper panel*) and the corresponding window function (*lower panel*). The three lines from bottom to top correspond to a 1%, 0.1% and 0.01% false alarm probability, respectively.

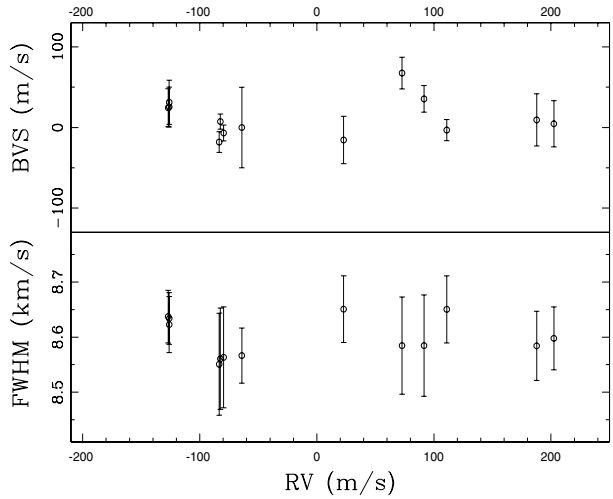

Fig. 3. *Upper panel*: bisector velocity span against the FEROS RVs. The BVS at each epoch was computed from the mean BVS in 11 different orders. The error bars correspond to the uncertainty in the mean. *Lower panel*: FWHM of the CCF versus the measured RVs. In this case we computed the mean value from three consecutive orders.

Table 4. Orbital parameters of HIP 105854 b.

Parameter	Value
P (days)	184.2 ± 0.5
K (m s^{-1})	178.1 ± 10.0
a (AU)	0.81 ± 0.03
e	0.02 ± 0.03
ω (deg)	343.2 ± 4.9
$M \sin i$ (M_J)	8.2 ± 0.2
T_0 (JD)	2 455 262.4 ± 2.4
γ_1 (m s^{-1})	14.4 ± 4.2
γ_2 (m s^{-1})	22.3 ± 9.0

to a smaller mass for HIP 105854 b (~7.4 M_J), while the orbital period and eccentricity remain unchanged. The derived orbital parameters are listed in Table 4. The offset velocities of FECH/CHIRON and FEROS data are also listed (γ_1 and γ_2, respectively). Additionally, Fig. 2 shows the Lomb-Scargle periodogram (Scargle 1982) of the HIP 105854 RVs (upper panel). The three lines from bottom to top correspond to a false alarm probability of 1%, 0.1% and 0.01%, respectively. As can be seen there is a strong peak around 184 days. Also, the lower panel shows the periodogram of the window function. Clearly the peak observed in the RVs is not explained by a periodicity in the sampling.

Since the period of the signal is close to half a year, we scrutinized in great detail the calculation of the barycentric correction that could lead to such an artifact. We found no problem in the coordinates or dates. Moreover, we computed the barycentric correction using two independent codes (based on FORTRAN and IDL, respectively), which yielded velocities that agree within 1 m s^{-1} for this planet and have found no such periods in more than the 100 stars we are monitoring.

2.5. Line profile analysis and stellar photometric variability

To investigate the nature of the RV signal present in our data we have performed a line profile analysis and we studied the photometric variability of HIP 105854. Figure 3 shows the result of the line profile analysis. We included only FEROS data since the FECH and CHIRON spectra also contain the I_2 features. The bisector velocity span (BVS) and full width at half maximum (FWHM) of the CCF are plotted as as function of the measured radial velocities (upper and lower panel, respectively). The BVS values were computed for 11 different orders, giving rise to a mean BVS value at each observational epoch. Similarly, we computed the mean FWHM in three consecutive orders ($\Delta\lambda \sim 500$ Å), since the width of the CCF is wavelength dependent. The error bars correspond to the uncertainty in the mean of these two quantities. As can be seen in Fig. 3, our BVS and FWHM values are consistent with a flat line. This result shows that no mechanism causing line asymmetries seems to be responsible for the observed RV signal.

In addition, we computed stellar chromospheric activity, as described in Jenkins et al. (2008, 2011). The results are plotted in Fig. 4. As can be seen, no obvious correlation is present between the S-index and the measured RVs.

Finally, to study whether the observed period is due to rotational modulation we measured the rotational period of the host star. Based on the derived stellar radius and projected rotational velocity (see Jones et al. 2011) we obtain $P_R = 137 \pm 36$ days. It can be noted that the orbital and rotational periods depart by more than one sigma. Moreover, by assuming a mean inclination angle of $i = 45°$, the two values differ by more than 2 sigma. In addition, we analysed the HIPPARCOS photometric data of HIP 105854. This dataset consists of 62 reliable H_p observations (quality flag 0 or 1), taken between Julian dates 2 447 975.3 and 2 448 975.6. The photometric variability is at the 0.006 mag level, and no significant periodicity is observed in the LS periodogram. This level of variability in slowly rotating stars (such as HIP 105854) is well below the predicted photometric variations that are accompanied by a RV amplitude at the ~200 m s^{-1} (Hatzes 2002). We can therefore discard the presence of spots (at least at the time that the HIPPARCOS data were obtained), hence it is unlikely that rotational modulation is the mechanism responsible for the periodic RV signal observed in the HIP 105854 data.

3. The properties of planets around giant stars

So far, more than 50 planets have been detected around giant stars, which have revealed different properties than those

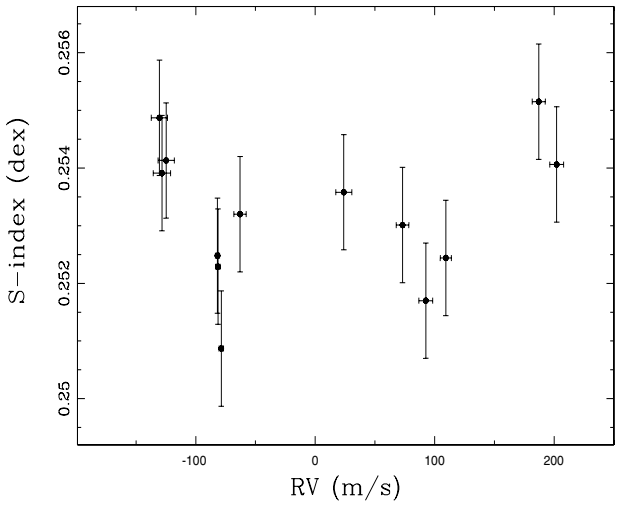

Fig. 4. Stellar chromospheric indicators (S-index) versus the measured radial velocities for HIP 105854. The S-index is computed following the procedure described in Jenkins et al. (2008, 2011).

orbiting solar-type stars. In this section, we review the semi-major axis, minimum mass and eccentricity distributions of these objects. Additionally, we discuss about the role of the stellar mass and stellar evolution on these properties.

3.1. Orbital distribution

After the detection of the first few planets around evolved stars, it was noticed that they are not found in orbits interior to ∼0.7 AU (e.g., Johnson et al. 2007; Sato et al. 2008). Nowadays, more than 100 exoplanets have been discovered around such stars (including subgiants), and the paucity of short-period systems is still present. Figure 5 (left) shows the minimum mass of planets (up to 13 M_J) as a function of the orbital distance, for planets around subgiant (blue triangles) and giant (red circles) stars, respectively. For comparison, the position of the planets around solar-type stars (0.7 $M_\odot > M_\star >$ 1.2 $M_\odot$) are overplotted (small black dots). The dotted lines correspond to a radial velocity amplitude of 30 m s^{-1} (assuming $M_\star$ = 1.5 $M_\odot$ and a = 1.0 AU, respectively), hence the planets above these lines should be easily detected by the current RV surveys. It can be seen that there is an absence of planets orbiting giant stars at orbital distances below ∼0.5 AU[2,3]. This observational result has been attributed to be due to the dynamical interaction between the host stars and their planets. Different authors have studied this effect, showing that close-in planets spiral inward due to the loss of orbital angular momentum, which is mainly transferred and dissipated in the stellar convective envelope (e.g., Livio & Soker, 1983; Rasio et al. 1996; Sato et al. 2008; Schröder & Connon Smith 2008; Villaver & Livio 2009; Kunitomo, et al. 2011). As a result of the tidal decay, close-in planets are not expected to be found, at least, around post-RGB stars. However, this theoretical prediction is far from being completely in agreement with the observed orbital properties of planets around giant stars. For instance, Villaver & Livio (2009) predict that the minimum orbital separation at which a planet survives around a 2 $M_\odot$ star is 2.1 AU and 2.4 AU for planets with 1 M_J and 3 M_J, respectively, which does not agree with the observational results, as shown in Fig. 5. This is because most of the planet-hosting giants are clump stars, thus most of them are core He-burning stars (i.e., post-RGB). However, based on a similar approach, Kunitomo et al. (2011) showed that the theoretical minimum survival distance for planets around giant stars, is in agreement with the observational results, also showing that the main differences with Villaver & Livio predictions arise in the stellar evolutionary models. In fact, different evolutionary models predict very different stellar radii during the final stage of the RGB phase. This is certainly the largest uncertainty in the tidal decay term, which is strongly dependent on the ratio of the stellar radius and the orbital distance.

It can be also seen in Fig. 5 that planets around subgiants reside on average at larger orbital distances than those orbiting giants stars, with the exception of the short period planets ($a \lesssim$ 0.2 AU). These close-in substellar objects are likely destroyed by the host star during the end of the RGB phase, when the stellar radius becomes larger than the orbital separation. In particular, there is an overabundance of planets around giant stars orbiting between ∼0.5 and 0.9 AU. Indeed, there are only two planets around subgiant stars in this region, in contrast to 16 of them orbiting giant stars, corresponding to ∼4% and ∼32% of the total population, respectively. This result might suggest that planets around giant stars move inward during the RGB and/or horizontal branch (HB) phase. Because of the effect of the tidal decay, planets around giant stars that reside between the survival limit and a maximum critical distance are expected to shrink their orbital radius. Therefore, as a result of the stellar evolution, these planets are expected to be absent in close-in orbits and on average closer than those around less evolved stars. On the other hand, planets that reside at much larger orbital distance avoid the strong tidal interaction and they increase their orbital radius due to the lower gravitational potential caused by the stellar mass loss. This process thus might explain the difference in the orbital distance of planets around giant stars and those orbiting subgiant stars that is observed in Fig. 5.

This interpretation, however, has to be taken with caution. In particular, the uncertainty in the mass and evolutionary status of the host stars might be biasing this result. Lloyd (2011, 2013) claimed that the mass of the planet-hosting subgiants and first ascending giant stars have been systematically overestimated or that many of such detections are actually false positives. If either of these is the actual case, then the previous argument is not valid, and hence the orbital properties of planets around subgiant and giant stars cannot be directly compared because their host stars comes from two different populations (mainly low-mass and intermediate-mass stars, respectively). In such a case, it is not possible to disentangle the effect of the stellar mass and disk properties (migration mechanism, dissipation timescale, etc.) from the stellar evolution. In addition, Bowler et al. (2010) showed that the period–mass distribution of planets around solar-type and intermediate-mass stars are different at the 4σ level. In particular, they showed that planets around subgiant stars with 1.5 $M_\odot < M_\star <$ 2.0 $M_\odot$ tend to reside at larger distances from the host star ($a >$ 1 AU) and that their occurrence rate is higher. Since the subgiants still have relatively small radii, this is not expected to be attributed to tidal decay, and hence it reveals a primordial different formation and evolution of planets around more massive stars. This result is incompatible with Lloyd's first alternative in the sense that if these subgiant stars are actually low-mass stars, then their planets should exhibit similar properties to those exhibited by systems around solar-type stars.

[2] HIP 13044 b was shown not to be a planet (Jones & Jenkins 2014).
[3] There is a planet candidate in a 6.2-days orbit detected via light curve variations (Lillo-Box et al. 2014).

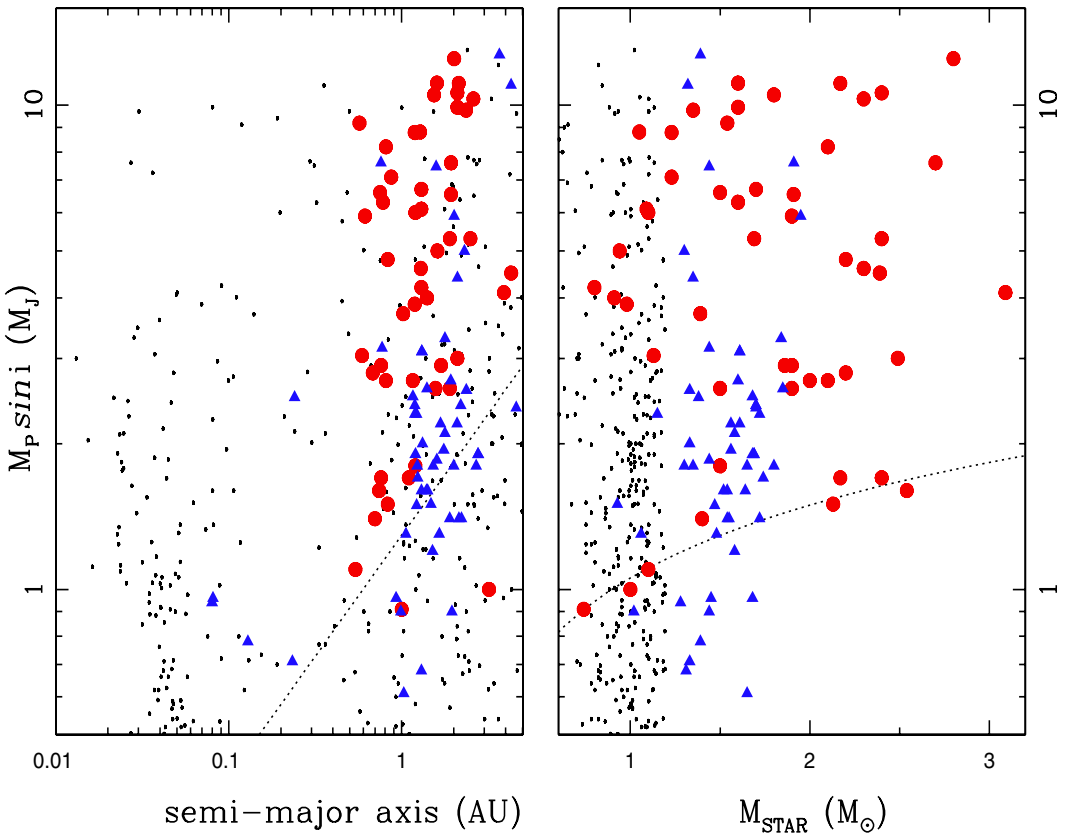

Fig. 5. Minimum mass of the planet versus the orbital distance and mass of the host star (*left and right panels*, respectively). The blue triangles and red filled circles correspond to subgiant and giant host stars, respectively. The small black dots show the position of known planets around solar-type stars. The dashed lines correspond to a RV amplitude of 30 m s^{-1}, for a planet orbiting a 1.5 $M_{\odot}$ star (*left panel*) and to an orbital distance of 1 AU (*right panel*).

3.2. Mass distribution

Although the current spectrographs, such as the High Accuracy Radial velocity Planet Searcher (HARPS; Mayor et al. 2003), allow us to reach a RV precision at the sub-m s^{-1} level, the detection of planets around evolved stars via the RV technique is restricted to gas giants, since stellar oscillations make the detection of RV signals below the ∼30 m s^{-1} level more difficult. However, it is still possible to study the properties of such massive planets, and compare them with the population of gas giants around solar-type stars.

The first indication of the peculiar mass distribution of planets around evolved stars was presented by Lovis & Mayor (2007) whom, based on a very restricted sample, suggested that there was an abnormally high fraction of massive planets and brown dwarfs around post-MS stars. Afterward, this result was confirmed by Döllinger et al. (2009), who showed that the giant planets around giant stars are more common and on average more massive than those detected in solar-type stars. This observational result is clearly observed in Fig. 5. As can be seen, most of the giant planets around giant stars are super planets ($M_{\rm p} \gtrsim 3\ M_{\rm J}$). This is in stark contrast to the mass distribution of giant planets around low-mass stars, since most of them have masses below ∼2 $M_{\rm J}$[4]. This result can be interpreted to be caused by the influence of the host star mass on the properties of substellar companions. It seems natural to expect that more massive stars have more massive and denser disks, from where massive planets are efficiently formed. However, it can be seen in Fig. 5 (right) that there is no dependence of the planet's mass with the stellar mass. Moreover, the mass distribution of planets around giant stars is completely different than for planets orbiting subgiants. To investigate the difference between the two distributions, let us consider only those planets around stars with $0.9\ M_{\odot} < M_{\star} < 2.0\ M_{\odot}$. A K-S test yields a null hypothesis probability of only 3×10^{-7}, meaning that the two datasets are drawn from different distributions.

Although it is difficult to interpret this result, it suggests that planets grow during the giant phase of the host star. One possibility is that planets accrete material directly from the stellar envelope or from the stellar wind during the RGB phase. These ideas have been studied from a theoretical point of view in the past. For instance, Livio & Soker (1983, 1984) showed that planets with $M_{\rm p} \gtrsim 13\ M_{\rm J}$ can survive inside the stellar envelope thus accreting a significant amount of mass. As a result, the planet ends up in a very close-in orbit and having a mass of ∼0.14 $M_{\odot}$. However , they also showed that smaller planets are either evaporated in the stellar envelope or they rapidly spiral inward and finally collide with the stellar core.

On the other hand, accretion from the stellar wind seems to be a plausible growing mechanism, since it is not expected to affect the planet's orbit during this process considerably. Duncan & Lissauer (2008) showed that the total amount of material hitting the planet during the entire RGB phase is only a fraction of the planet's mass, meaning that this mechanism cannot solely be responsible for this observational result. Spiegel & Madhusudhan (2012) confirmed the previous results, but they also showed that through this mechanism the planet can accrete

[4] Source: http://exoplanet.eu

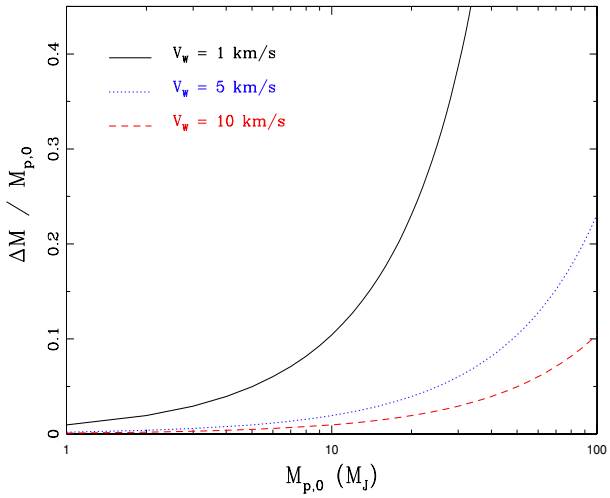

Fig. 6. Fractional amount of mass accreted by a planet as a function of its initial mass. The three horizontal lines correspond to wind velocities at the planet's position of 1, 5 and 10 km s^{-1}, respectively.

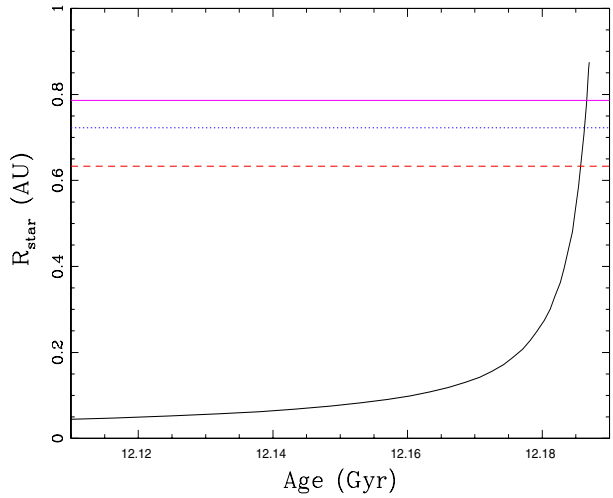

Fig. 7. Evolution of a 1 $M_\odot$ star radius, at the end of the RGB phase (from Salasnich et al. 2000 models). The three horizontal lines (from bottom to top) show the Roche radius of the star in the presence of a planet at 1 AU, with masses of 50, 10 and 1 M_J, respectively.

a significant amount of mass in its atmosphere, thus modifying its composition. We performed similar calculations, considering Bondi-Hoyle accretion (Bondi & Hoyle 1944), without planet evaporation. We integrated the stellar mass-loss formula given by (Reimers 1975), assuming a spherical distribution, through the entire RGB phase, using a 1.0 $M_\odot$ star model from Salasnich et al. (2000). We used a value of $\eta = 2.6 \times 10^{-13}$, so that the total mass lost during the RGB is 0.33 $M_\odot$, as predicted by Schröder & Connon Smith (2008). The orbital distance of the planet was fixed to 1.0 AU. At each time step we updated the mass of the planet. Figure 6 shows the normalized total accreted mass as a function of the initial mass of the planet. The three lines correspond to wind velocities at the planet's position of 1, 5 and 10 km s^{-1}, respectively. As can be seen, a giant planet ($M_p \lesssim 10\ M_J$) is able to accrete a significant amount of mass only for very low-wind-velocity ($\sim$1 km s^{-1}). For higher wind velocities ($\gtrsim$5 km s^{-1}), the total accreted mass is negligible. This result is also valid for planets around intermediate-mass stars, since the mass-loss rate is even lower. However, the total accreted mass by the planet might be significantly higher in the case of non-spherical or enhanced mass-loss (e.g., Tout & Eggleton 1988). If the star loses mass preferentially through a disk aligned with the planet's orbital plane, then the density of the wind at the planet's position is much higher. On the other hand, an enhanced mass-loss rate, driven for instance by the deposition of angular momentum in the stellar envelope by other planets in the system (Soker 1998), might lead to a much higher total accreted mass. For more massive substellar objects ($M \gtrsim 50\ M_J$), the accretion rate is much higher and thus a substellar companion might be able to accrete a total of several Jupiter masses at wind velocities of 5–10 km s^{-1} and at an orbital distance up to a few AU. Moreover, in the low-wind-velocity regime, these objects accrete enough material to become a low-mass star. This result should be investigated in more detail in the future, since this mechanism can be responsible for the lack of massive brown dwarfs in relatively close-in orbits around post-MS stars.

A third possibility is that the star overfills its Roche lobe, thus directly transferring material to the planet. Figure 7 shows the evolution of the stellar radius (1 $M_\odot$ model described above), at the end of the RGB phase. The solid, dotted and dashed lines correspond to the Roche radius (see Eggleton 1983) of the star in the presence of an orbiting planet at 1 AU with $M_P = 1, 10$ and 50 M_J, respectively. The star overfills its Roche lobe before reaching the tip of the RGB phase, meaning that there is material that is transferred directly from the stellar envelope to the planet. Also, as can be seen in Fig. 7, the radius of the star at this stage is comparable in size with the orbital distance, which also is accompanied by a strong tidal effect that would eventually lead to the planet engulfment. However, if the tidal decay is weak enough so that the planet avoids engulfment, the planet can accrete material from the wind and later on via direct mass transfer, reducing its orbital distance (because of the accretion process and by tidal decay) and increasing its mass. This scenario might explain the peculiar orbital and mass distributions revealed by planets orbiting giant stars.

Finally, these planets might be the remnants of either brown dwarfs or low-mass stellar companions that lost their envelope during the common-envelope phase. The main problem with this idea is that this process leads to a significant loss of the stellar envelope, and thus to the formation of an extreme horizontal branch star (Soker 1998; Han et al. 2002).

3.3. Eccentricity

One of the most surprising properties of exoplanets is their relatively large orbital eccentricity. Figure 8 shows the eccentricity as a function of planets semi-major axis. The symbols are the same as in Fig. 5. As can be seen in Fig. 8, there are two distinctive populations: planets orbiting interior to ~0.1 AU, which present relatively low eccentricities, and those at larger orbital distances, where there are many highly eccentric systems.

The origin of the large eccentricities observed in extrasolar planets is puzzling, since the eccentricity is predicted to be efficiently damped during the early planet formation stage via interaction of the planet with the gaseous disk (e.g., Artymowicz 1993; Tanaka & Ward 2004). As a result of this process, planets are expected to have nearly circular orbits after their formation. Different mechanisms might be responsible for pumping-up the orbital eccentricity, such as planet-planet interactions (e.g., Lin & Ida 1997; Marzari & Weidenschilling 2002) and planet-star interactions (e.g., Holman et al. 1997; Zakamska & Tremaine 2004). In this context, the low e values exhibited by the short-period systems are likely explained by the subsequent effect of

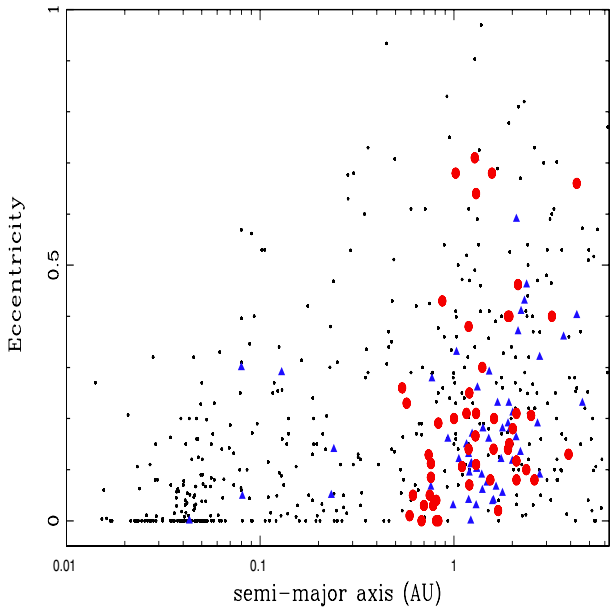

Fig. 8. Planet's eccentricity against the orbital distance. The blue triangles and red filled circles correspond to subgiant and giant host stars, respectively. The small black dots show the position of known planets around solar-type stars.

tidal circularization (e.g., Goldreich & Soter 1966; Rasio et al. 1996; Jackson et al. 2008), similar to what is seen in short period binary stars (Duquennoy & Mayor 1991; Verbunt & Phinney 1995).

Additionally, it seems that planets around post-MS stars have lower eccentricities than those orbiting MS stars. Let us consider the region between $a \sim 0.5$–3.0 AU, where most of the planets around evolved stars reside. While 32% of them have $e \leq 0.1$, only 19% of the planets around solar-type stars exhibit such low eccentricities. Moreover, considering e up to 0.2, we obtain a fraction of 70% for planets around subgiants, 64% for planets orbiting giants and 38% for system hosted by solar-type stars. These differences are significant and point out a different eccentricity distribution between planets around solar-type and post-MS stars. In fact, considering only the exoplanets orbiting in the above mentioned region, a K-S test gives a probability of 5.1×10^{-4} that the eccentricities of planets around giant stars and solar-type stars are drawn from the same distribution. Similarly, when the subgiants and solar-type host stars are compared, the K-S test yields a probability of 2.1×10^{-4}.

This observational fact might be interpreted as the result of tidal circularization, especially for giants stars, which have much larger radii than solar-type stars. In fact, although previous works included only the effect of tides in the planets, neglecting the influence of tides in the star, Jackson et al. (2008) showed that this term, which is strongly dependent on the stellar radius, might reduce the circularization timescale considerably. In this scenario however, the planets around subgiant stars should present larger eccentricities, because of their still relatively small radii and the short timescales involved.

On the other hand, this result might be telling us that a significant fraction of the MS star systems are actually multiplanets systems with circular orbits, which are misinterpreted as eccentric single planets (Anglada-Escude et al. 2010; Wittenmyer et al. 2012), especially when they are in resonant orbits (e.g., Jenkins et al. 2013b).

Last, since most of the planet-hosting evolved stars are more massive than solar-type stars, the low e values observed in planets around these stars might be explained by a different formation scenario. For instance, if multiplanets systems are not efficiently formed in disks surrounding more massive stars, then the gravitational perturbation between planets is strongly reduced. As a consequence, no significant enhancement of the planet's eccentricity by planet-planet interactions would be possible.

4. Summary and conclusions

We have reported the discovery of a substellar object in the planetary mass regime around the RGB star HIP 105854. The main orbital properties of the planet are the following: $M_{\rm p} \sin i = 8.2 \pm 0.2\ M_{\rm J}$; $P = 184.2 \pm 0.5$ days; $e = 0.02 \pm 0.03$. This is the second planet detected during our survey and adds up to a growing population of substellar companions that have been detected around evolved stars.

Based on the properties of more than 100 planets around post-MS stars, we have discussed the effect of the host star evolution on the orbital and mass distributions of such objects. We have shown that the planets around giant stars tend to reside at smaller orbital distances than those around subgiant stars. While most of the planets around subgiant stars have semi-major axes greater than ~1 AU, there is an overabundance of planets around giant stars orbiting between ~0.5–0.9 AU. This observational result might be explained in part due to the loss of angular momentum of planets during the RGB phase. In addition, short period planets are expected to be engulfed by the host star during the RGB phase, since the radius of the star becomes larger than the orbital distance at the end of the RGB phase, and that is why they are present only around subgiant stars and not around giant stars.

We also showed that the minimum mass distributions of planets around subgiant and giant stars are completely different, and that there is no dependence on the mass of the host star. This observational result suggests that there is an evolutionary effect and thus the planets grow during the RGB or HB phase. We proposed different mechanisms such as accretion from the stellar wind and mass transfer after the host star overfills its Roche lobe, which might explain some of the observational properties of these systems. Other possibilities, such a planet mergers, should be also considered.

Finally, we studied the eccentricity of planets around post-MS stars. We showed that on average they present lower eccentricity when compared to solar-type host stars. The explanation of this observational fact is uncertain, particularly because no significant difference is observed between planets around subgiant and giant stars. Probably the formation and evolution of planetary systems that are formed around more massive stars depart from the systems orbiting low-mass stars.

Acknowledgements. M.J. acknowledges financial support from Fondecyt Projects #3140607 and #1120299. P.R. acknowledges financial support from Fondecyt through grant #1120299 and Conicyt-PIA Anillo ACT1120. J.J. acknowledges funding by Fondecyt through grant 3110004, the GEMINI-CONICYT FUND and from the Comité Mixto ESO-GOBIERNO DE CHILE. M.J., J.J., and P.R. also acknowledge support from BASAL PFB-06 (CATA).

References

Anglada-Escude, G., Lopez-Morales, M., & Chambers, J. E. 2010, ApJ, 709, 168
Artymowicz, P. 1993, ApJ, 419, 166
Bondi, H., & Hoyle, F. 1944, MNRAS, 104, 273
Boss, A. 1997, Science, 276, 1836

Bowler, B. P., Johnson, J. A., Marcy, G. W., et al. 2010, ApJ, 709, 396
Butler, R. P., Marcy, G. W., Williams, E., et al. 1996, PASP, 108, 500
Demarque, P., Woo, J., Kim, Y., & Yi, S. K. 2004, ApJS, 155, 667
Döllinger, M. P., Hatzes, A. P., Pasquini, L., Guenther, E. W., & Hartmann, M. 2009, A&A, 505, 1311
Duncan, M. J., & Lissauer, J. J. 1998, Icarus, 134, 303
Duquennoy, A., & Mayor, M. 1991, A&A, 248, 485
Eggeleton, P. P. 1983, ApJ, 268, 368
Fischer, D. A., & Valenti, J. 2005, ApJ, 622, 1102
Frink, S., Quirrenbach, A., Fischer, D., Röser, S., & Schilbach, E. 2001, PASP, 113, 173
Goldreich, P., & Soter, S. 1966, Icarus, 5, 375
Gonzalez, G. 1997, MNRAS, 285, 403
Han, Z., Podsiadlowski, Ph., Maxted, P. F. L., Marsh, T. R., & Ivanova, N. 2002, MNRAS, 336, 449
Hatzes, A. P. 2002, Astron. Nachr., 323, 392
Holman, M., Touma, J., & Tremaine, S. 1997, Nature, 386, 254
Jackson, B., Greenberg, R., & Barnes, R. 2008, ApJ, 678, 1396
Jenkins, J. S., Jones, H. R. A., Pavlenko, Y., et al. 2008, A&A, 485, 571
Jenkins, J. S., Murgas, F., Rojo, P., et al. 2011, A&A, 531, L8
Jenkins, J. S., Jones, H. R. A., Tuomi, M., et al. 2013a, ApJ, 766, 67
Jenkins, J. S, Tuomi, M., Brasser, R., Ivanyuk, O., & Murgas, F. 2013b, ApJ, 771, 41
Johnson, J. A., Fischer, D. A., Marcy, G. W., et al. 2007, A&A, 665, 785
Jones, M. I. 2013, Ph.D. Thesis, Universidad de Chile
Jones, M. I., & Jenkins, J. S. 2014, A&A, 562, A129
Jones, M. I., Jenkins, J. S., Rojo, P., & Melo, C. H. F. 2011, A&A, 536, A71
Jones, M. I., Jenkins, J. S., Rojo, P., Melo, C. H. F., & Bluhm, P. 2013, A&A, 556, A78
Kaufer, A., Stahl, O., Tubbesing, S., et al. 1999, The Messenger, 95, 8
Kennedy, G. M., & Kenyon, S. J. 2008, ApJ, 673, 502
Kunitomo, M., Ikoma, M., Sato, B., et al. 2011, ApJ, 737, 66
Lillo-Box, J., Barrado, D., Moya, A., et al. 2014, A&A, 562, A109
Lin, D. N. C., & Ida, S. 1997, ApJ, 477, 781
Livio, M., & Soker, N. 1983, AJ, 125, 12
Livio, M., & Soker, N. 1984, MNRAS, 208, 763
Lloyd, J. P. 2011, ApJ, 739, 49
Lloyd, J. P. 2013, ApJ, 774, 2
Lovis, C., & Mayor, M. 2007, A&A, 472, 657
Marzari, F., & Weidenschilling, S. J. 2002, Icarus, 156, 570
Massarotti, A., Latham, D., Stefanik, R. P., & Fogel, J. 2008, AJ, 135, 209
Mayor, M., Pepe, F., Bouchy, F., et al. 2003, The Messenger, 114, 20
Meschiari, S., Wolf, A. S., Rivera, E., et al. 2009, PASP, 121, 1016
Mortier, A., Santos, N. C., Sousa, S. G., et al. 2013, A&A, 557, A70
Pasquini, L., Döllinger, M. P., Weiss, A., et al. 2007, A&A, 473, 979
Queloz, D., Casse, M., & Mayor, M. 1999, ASP Conf. Ser., 185, 13
Randich, S., Gratton, R., Pallavicini, R., Pasquini, L., & Carretta, E. 1999, A&A, 348, 487
Rasio, F. A., Tout, C. A., Lubow, S. H., & Livio, M. 1996, ApJ, 470, 1187
Reimers, D. 1975, Mem. Soc. Roy. Sci. Liège, 8, 369
Salasnich, B., Girardi, L., Weiss, A., & Chiosi, C. 2000, A&A, 361, 1023
Santos, N. C., Israelian, G., & Mayor, M. 2001, A&A, 373, 1019
Sato, B., Kambe, E., Takeda, Y., et al. 2005, PASJ, 57, 97
Sato, B., Izumiura, H., Toyota, E., et al. 2008, PASJ, 60, 539
Scargle, J. D. 1982, ApJ, 263, 835
Schröder, K.-P., & Connon Smith, R. 2008, MNRAS, 386, 155
Schuler, S. C., Kim, J. H., Tinker, M. C., & King, J. R. 2005, ApJ, 632, 131
Soker, N. 1998, AJ, 116, 1308
Spiegel, D. S., & Madhusudhan N. 2012, ApJ, 756, 132
Tanaka, H., & Ward, W. R. 2004, ApJ, 602 388
Tokovinin, A., Fischer, D. A., Bonati, M., et al. 2013, PASP, 125, 1336
Tout, C. A., & Eggleton, P. P. 1988, MNRAS, 231, 823
Verbunt, F., & Phinney, E. S. 1995, A&A, 296, 709
Villaver, E., & Livio, M. 2009, ApJ, 705, 81
Wittenmyer, R. A., Horner, J., Tuomi, M., et al. 2012, ApJ, 753, 169
Zakamska, N. L., & Tremaine, S. 2004, AJ, 128, 869